Marine Geology 266 (2009) 198–211

Contents lists available at ScienceDirect

Marine Geology

journal homepage: www.elsevier.com/locate/margeo

A late Miocene–early Pliocene Antarctic deepwater record of repeated iron reduction events

Daniel A. Hepp [a,*], Tobias Mörz [a,b], Christian Hensen [c], Thomas Frederichs [a], Sabine Kasten [b,d], Natascha Riedinger [e], William W. Hay [f]

[a] Department of Geosciences, University of Bremen, P.O. Box 330440, 28334 Bremen, Germany
[b] MARUM-Center for Marine Environmental Sciences, University of Bremen, P.O. Box 330440, 28334 Bremen, Germany
[c] Leibniz Institute of Marine Sciences at the University of Kiel (IFM-GEOMAR), Wischhofstrasse 1-3, 24148 Kiel, Germany
[d] Alfred Wegener Institute for Polar and Marine Research (AWI), Am Handelshafen 12, 27570 Bremerhaven, Germany
[e] Max-Planck-Institute for Marine Microbiology, Celsiusstrasse 1, 28359 Bremen, Germany
[f] Department of Geological Sciences, University of Colorado, Boulder, Colorado 80309, USA

ARTICLE INFO

Article history:
Received 15 February 2008
Received in revised form 7 August 2009
Accepted 11 August 2009
Available online 21 August 2009

Communicated by G.J. de Lange

Keywords:
ice sheet dynamic
magnetic susceptibility minima Zone
ODP Site 1095
Pliocene warming
Antarctic Peninsula

ABSTRACT

In this study we present a late Miocene–early Pliocene record of sixty-four zones with prominent losses in the magnetic susceptibility signal, taken on a sediment drift (ODP Site 1095) on the Pacific continental rise of the West Antarctic Peninsula. The zones are comparable in shape and magnitude and occur commonly at glacial-to-interglacial transitions. High resolution records of organic matter, magnetic susceptibility and clay mineral composition from early Pliocene intervals demonstrate that neither dilution effects nor provenance changes of the sediments have caused the magnetic susceptibility losses. Instead, reductive dissolution of magnetite under suboxic conditions seems to be the most likely explanation. We propose that during the deglaciation exceptionally high organic fluxes in combination with weak bottom water currents and prominent sediment draping diatom ooze layers produced temporary suboxic conditions in the uppermost sediments. It is remarkable that synsedimentary suboxic conditions can be observed in one of the best ventilated open ocean regions of the World.

1. Introduction

The latest Miocene–early Pliocene is thought to be a period of warm climate conditions in the Southern Ocean (Kennett and Hodell, 1995), which is consistent with a globally enhanced primary productivity (Dickens and Owen, 1999; Diester-Haass et al., 2005; Farrell et al., 1995). Changes in global climate and ocean circulation systems led to an important transition in global nutrient cycling, which left an imprint on opal deposition records in marine sediments. Causes for this late Neogene global change are currently under debate for major tectonic, oceanographic and cryosphere events (closure of the Isthmus of Panama, the establishment of the modern thermohaline circulation, the evolution of the Northern Hemisphere ice sheet, and the development of the West Antarctic Ice Sheet = WAIS; Cortese et al., 2004; Haug and Tiedemann, 1998; Kennett and Barker, 1990; Knorr and Lohmann, 2003). These events altered the strength and flow directions within the global circulation pattern, and also affected the meridional partitioning of nutrients, essential to opal-producing organisms. The global evidence for enhanced primary productivity and accumulation of biogenic components in the sediment during the latest Miocene–early Pliocene has been coined the 'biogenic bloom' hypothesis (Cortese et al., 2004; Dickens and Owen, 1999; Diester-Haass et al., 2005; Farrell et al., 1995; Hermoyian and Owen, 2001).

Ice has been present on Antarctica since the Eocene/Oligocene transition (Zachos et al., 2001). Since the late Miocene (~10 Ma) West Antarctica has been covered by a waxing and waning ice sheet that periodically extended to the shelf edge (Kennett and Hodell, 1995). The sedimentary response to Antarctic Peninsula Ice Sheet (APIS) dynamics and changes in the regional oceanographic realm during the latest Miocene–early Pliocene warming phase is well documented in distal records from the Pacific continental rise off the Antarctic Peninsula (Barker and Camerlenghi, 2002; Pudsey, 2002). Such changes, especially enhanced primary productivity and accumulation of biogenic components, are reflected in paleoenvironmental proxies, e.g. the magnetic signal in the sedimentary record.

Prominent losses of the magnetic susceptibility signal have been reported in studies of the South Atlantic (Funk et al., 2004a; ODP Leg 165 Shipboard Scientific Party, 1997), the western South Atlantic (Garming et al., 2005; Hensen et al., 2003; Riedinger et al., 2005), the North Pacific (Dickens and Owen, 1996; Karlin, 1990; Novosel et al., 2005; Weeks et al., 1995), the Southwest Pacific (ODP Leg 181 Shipboard Scientific Party, 1999), the East Antarctic continental

* Corresponding author. Tel.: +49 421 218 65844; fax: +49 421 218 65810.
E-mail address: dhepp@uni-bremen.de (D.A. Hepp).

0025-3227/$ – see front matter © 2009 Elsevier B.V. All rights reserved.
doi:10.1016/j.margeo.2009.08.006

margin (Florindo et al., 2003), and the western Antarctic Peninsula (Brachfeld et al., 2002a,b; Hepp et al., 2006; Sagnotti et al., 2001). The loss of the magnetic susceptibility signal may have a variety of reasons and characteristics, e.g. sedimentary processes like dilution effects (Diekmann et al., 2000), changes in provenance of the source material and composition of the supplied sediments (Brachfeld et al., 2002a; Hillenbrand and Ehrmann, 2002, 2005; Lucchi et al., 2002b; Sagnotti et al., 2001), or, post-depositional magnetite dissolution driven either by dissimilatory iron reduction (Funk et al., 2004a; Passier et al., 1999; Thomson et al., 1998) or by hydrogen sulfide produced during the anaerobic oxidation of methane (Hensen et al., 2003; Kasten et al., 2003; Riedinger et al., 2005).

In our sedimentary and oceanographic study on ODP Site 1095 (Pacific continental margin of the Antarctic Peninsula) we have compiled a new late Miocene–early Pliocene record of repeated magnetic susceptibility losses to (1) give an explanation of their origin, (2) outline the mode and the impact of a high dynamic APIS on primary productivity and bottom water ventilation, and (3) discuss the imprint of global climate signals on our Antarctic Peninsula record.

We analyzed three shorter Pliocene sequences across zones with prominent losses of the magnetic susceptibility signal (171.50–163.50, 124.50–117.50, and 107.50–101.50 meter composite depth = mcd). In more detail we present the pattern across the interval 107.50–101.50 mcd.

2. Regional setting

The Pacific continental margin of the Antarctic Peninsula is part of a complex glacial sedimentary system. The system comprises lobes and troughs on the outer shelf, a steep slope, and deep-sea channels separating a series of twelve sedimentary drifts on the upper continental rise (Fig. 1; Pudsey and Camerlenghi, 1998; Rebesco et al., 2002; Uenzelmann-Neben, 2006). The channel system is maintained by the interplay of downslope turbidity currents and South-West flowing along-slope bottom currents (Hillenbrand et al., 2008; Pudsey and Camerlenghi, 1998). Drift 7 is one of the largest sediment mounds located west of the Antarctic Peninsula. Its asymmetrical shape, with a gentle North-East side and a steep South-West side, is similar to other sediment drifts in this area. The late Miocene–early Pliocene drift build-up was dominated by glacially driven turbidity currents and interglacial pelagic settling (Hepp et al., 2006; Pudsey, 2002; Uenzelmann-Neben, 2006). The distal part of Drift 7 was drilled during Ocean Drilling Program (ODP) Leg 178 (ODP Leg 178 Shipboard Scientific Party, 1999) and SEDANO projects (Lucchi et al., 2002a,b; Sagnotti et al., 2001). The ODP Site 1095 sediment cores represent a continuous proximal marine sedimentary record of APIS dynamics from late Miocene to Holocene (~10 Ma; Fig. 2).

3. Methods

The applied methods can be summarized as a combined sedimentological and geochemical approach. We re-opened all relevant cores of ODP Site 1095 for re-description and sedimentological analyses of glacial and interglacial variability and occurrences of diatom oozes, ice rafted debris (IRD) and silt layers. We analyzed a suite of sedimentological, geophysical and geochemical parameters, which are already presented in Hepp et al. (2006), and present new IRD gravel counts, magnetic susceptibility, X-ray fluorescence spectrometry (XRF), clay mineral, biogenic silica ($BSiO_2$) and total organic carbon (TOC) data.

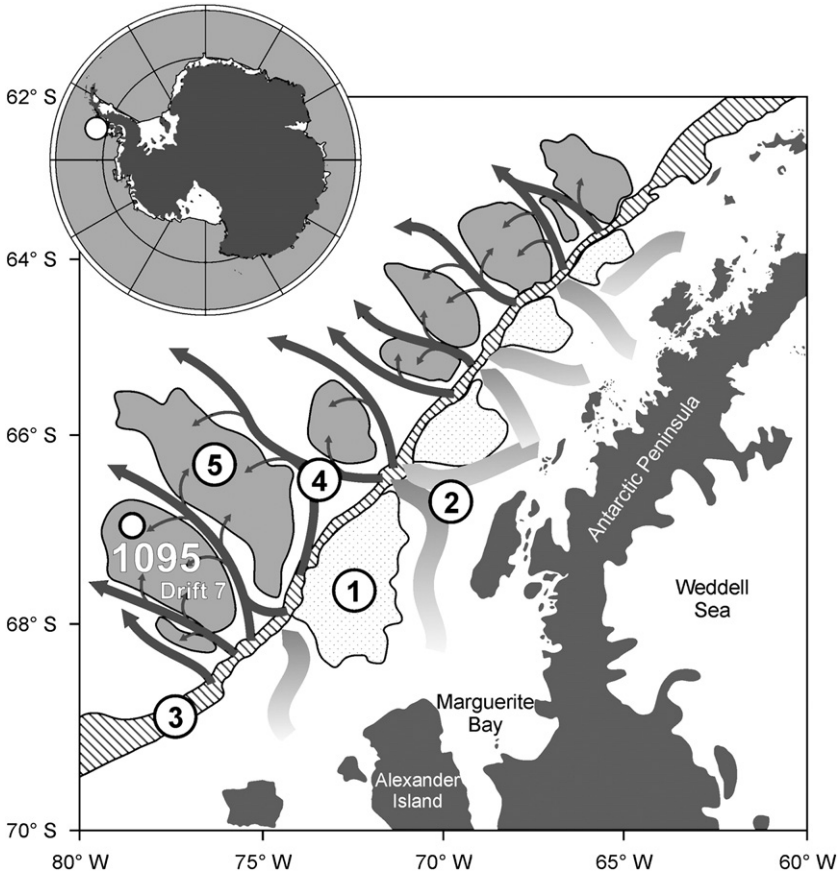

Fig. 1. Drawing of the Pacific continental margin off the Antarctic Peninsula. The map shows a glacial driven sediment feeder system of (1) lobes and (2) troughs on the outer shelf, (3) an steep slope, (4) deep-sea channels, (5) a series of sediment drifts on the continental rise, and the location of ODP Site 1095 on the distal part of Drift 7. The light arrows marks supposed ice stream pathways. The dark arrows show possible pathways of gravity flows and overbank 'turbidity' currents (modified after Lucchi et al., 2002a; Rebesco et al., 2002).

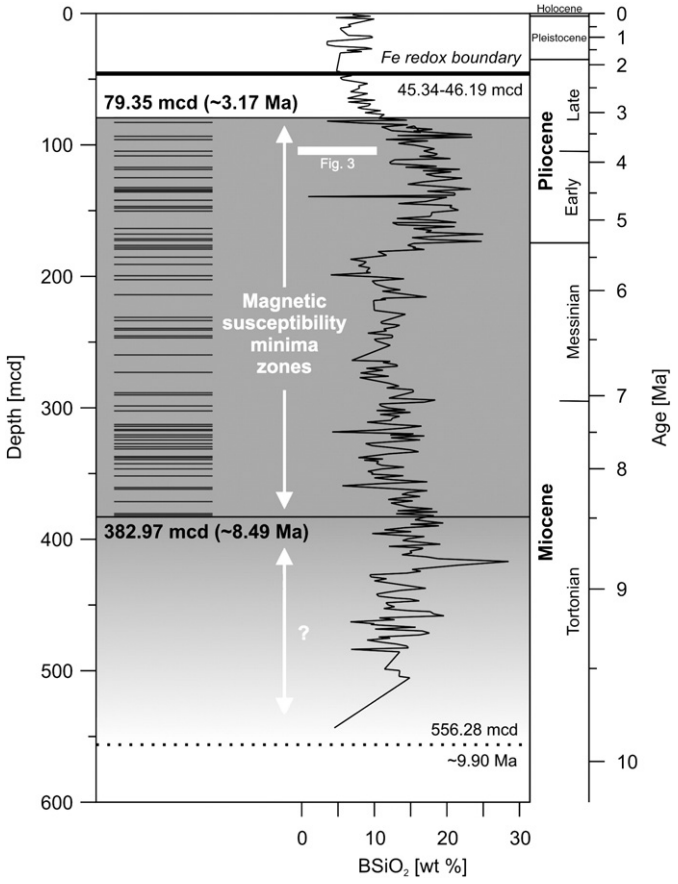

Fig. 2. Schematic representation of core ODP Site 1095 (0–556.28 mcd), the 64 MSMZs (382.97–79.35 mcd; 'bar code') and present positions of Fe^{2+}/Fe^{3+}-redox boundary (45.34–46.19 mcd). The biogenic opal ($BSiO_2$; Hillenbrand and Fütterer, 2002) indicates the biological productivity since late Miocene. The composite depth scale is given in Barker (2002). The linear interpolated age model is based on magnetostratigraphic–biochronologic tie-points given in Acton et al. (2002) and Iwai et al. (2002).

Silt layers (Fig. 3a) and IRD gravels (counts of >1 cm diameter/10 cm grid; Fig. 3b) were counted and mapped on the basis of X-ray core images. The digital X-ray images were made from selected core sections using medical 'Fluorospot compact' equipment for radiography.

Magnetic susceptibility (κ; Fig. 3c) was measured with a shipboard whole-core multisensor core logger during ODP Leg 178 (ODP Leg 178 Shipboard Scientific Party, 1999). This fast, high-resolution measuring method allowed a firsthand identification and mapping of zones with a loss in the magnetic susceptibility signal (Hepp et al., 2006). New single measurements ($\kappa_{distinct}$; Fig. 3d) on forty samples from core section 107.5–101.5 mcd were carried out with a 'KappaBridge KLY-2' at University of Bremen. The $\kappa_{distinct}$ were determined for the total sample and the fine fraction (<63 μm). The values for the coarse fraction were calculated by subtracting the fine fraction from total sample values. In addition we performed low-temperature magnetic measurements (thermal demagnetization of a 5-T low-temperature remanence) after field (FC) and zero-field cooling (ZFC) and high-field (7 T) magnetic hysteresis loops at room temperature on a subset of six samples. The measurements were performed on a 'Quantum Design MPMS XL-7' at University of Bremen.

A suite of elements, e.g. manganese (Fig. 3e), iron (Fig. 3f, Appendix A), titanium and barium (Fig. 3k), were quantitatively analyzed (intervals 171.5–163.5, 124.5–117.5, and 107.5–101.5 mcd) at the Bremen IODP Core Repository using an 'AvaaTech XRF scanner'. Single XRF measurements on molten sub-samples were conducted to convert the XRF scanner counts to calibrated weight % data by means of a simple linear regression. We point out that this attempt neglects the constant-sum constraint on concentrations. In view of this problem, XRF core-scanner data are widely regarded as semi-quantitative only (Weltje and Tjallingii, 2008). The conservative element aluminum was used to estimate the biogenic barium (Ba_{bio}) fraction by subtracting the concentration of terrigenous barium from the total barium concentration (Dymond et al., 1992) with a $Ba/Al_{aluminosilicate}$ ratio of 0.0048 as defined by Pudsey (2000, core 106).

We analyzed ten samples from core section (107.5–101.5 mcd) using the standard X-ray diffraction analysis (XRD) combined with a quantification method of mineral phases based on the full-pattern method QUAX (Vogt et al., 2002). The derived absolute clay mineral concentrations are of high precision (Vogt et al., 2002), but not directly comparable to relative clay mineral percentages by means of empirical factors (Biscaye, 1965).

The biogenic opal content shown in Figs. 2 and 7d was adapted from Hillenbrand and Fütterer (2002). We refined the opal data set by 50 additional biogenic silica analyzes (Fig. 3h) from core section 107.5 to 101.5 mcd to document the opal variability at the terminations and to differentiate the opal content of turbidity and hemipelagic sediments. The homogenized dry bulk samples were analyzed using an automated leaching technique after Müller and Schneider (1993). Total organic carbon data (Fig. 7e) were provided by Wolf-Welling et al. (2002). Forty additional TOC data points (Fig. 3i) and total sulfur content (Fig. 3j) were used for the interpretation on short time-scales. The TOC and sulfur measurements were carried out using a 'LECO CS-125 analyzer'. Core depth follows the ODP nomenclature and is given in revised mcd (Barker, 2002).

We used near surface porosity values based on shipboard index samples for de-compaction and reconstruction of the original depositional interval length of zones with magnetic susceptibility loss following Terzaghi's compaction theory (Azizi, 2000, p. 170, equ. 4.1; Fig. 7b). To overcome the high glacial and interglacial scatter in Fe/κ (Fig. 7c) and total organic carbon (Fig. 7e) data, moving average and Hilbert transforms were applied for a better visualization of the long-term trends.

4. Results and discussion

4.1. Identification of magnetic susceptibility minima zones

We report on the identification of sixty-four zones with prominent losses of the magnetic susceptibility signal, which are comparable in shape, magnitude and value. These zones, in the following referred to as magnetic susceptibility minima zones (MSMZ), are characterized by a U-shaped minimum of about one order of magnitude in magnetic susceptibility (MSMZ average of 38 10^{-5} SI versus total magnetic susceptibility average of 315 10^{-5} SI) and a lack of variance in the bottom part. For our analysis U-shaped, flat based magnetic susceptibility zones with values less than $100*10^{-5}$ SI were classified as MSMZ. Comparable late Miocene zones with a loss in the magnetic susceptibility signal are presented but not further discussed by Pudsey (2002, Fig. 8).

MSMZ occur in ODP Site 1095 data between 79.35 mcd (~3.17 Ma) and 382.97 mcd (~8.49 Ma; Fig. 2). The 300 m long core sequence represents a period of ~5 my, from late Miocene to early Pliocene. The upper termination of the MSMZ interval is very well defined in a late Pliocene core section of excellent quality. Below 382.97 mcd increased sediment compaction and alteration of biogenic opal-A to opal-CT or cryptocrystalline quartz (Volpi et al., 2003) led to a decrease in core quality that prevented the mapping of MSMZs with simple threshold criteria.

4.2. Magnetic susceptibility minima zones on the scale of glacial cycles

Fig. 3 shows a combination of lithological, geophysical and geochemical data from ODP Site 1095 core interval between 107.50 and 101.50 mcd (Overview data for the other two sections are given in Appendix A). The interval consists of clayey laminated silt layer-rich

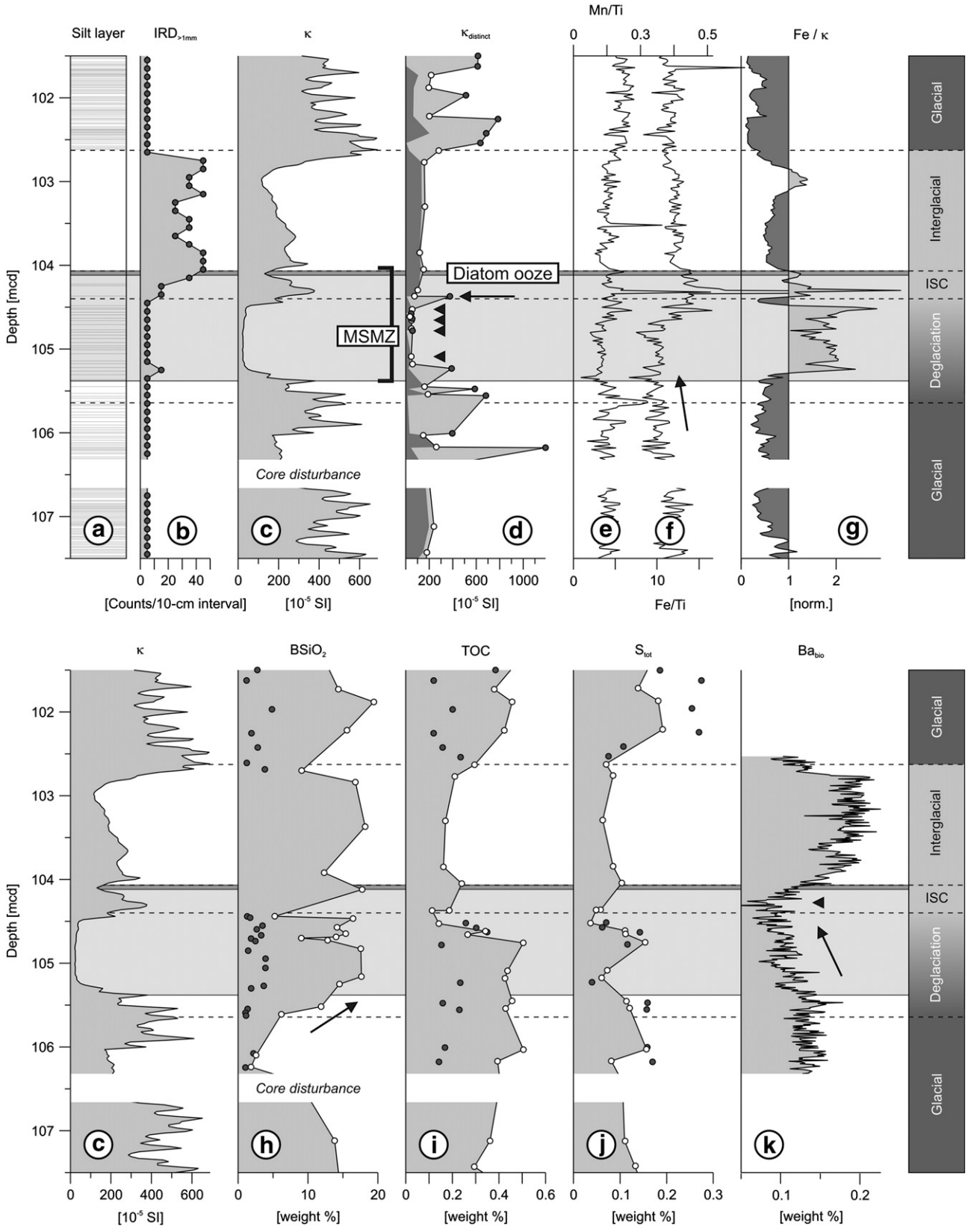

Fig. 3. Example of a MSMZ (105.28 and 104.48 mcd) in the context of a complete glacial–interglacial cycle (107.50 and 101.50 mcd, ODP Leg 178 Site 1095B-3H4 to 4H1): (a) absolute position of silt layers, (b) number of IRD gravel (>1 cm/10-cm grid), magnetic susceptibility (κ) from (c) shipboard logging data and (d) single measurements (light shading = grain-size coarse fraction >63 μm, dark shading = grain-size fine fraction <63 μm), (e) Mn/Ti ratio and (f) Fe/Ti ratio from X-ray fluorescence spectrometry (XRF) logging, (g) normalized Fe/κ ratio, (h) biogenic silica (opal), (i) total organic carbon and (j) total sulfur from single samples, and (k) biogenic barium from XRF logging (Open circles = samples from hemipelagic sediments, solid circles = samples from silt layers (<63 μm), dark bar = diatom ooze layer, shaded area = MSMZ, dashed lines = boundaries of glacial stages, arrows = as given in the text).

and silt layer free intervals (Fig. 3a) with high diatom abundance of up to 30% (ODP Leg 178 Shipboard Scientific Party, 1999) and IRD in the silt layer-free parts (Fig. 3b). These sedimentation patterns are thought to reflect a full glacial–interglacial cycle with characteristic transitions at 104.72 and 102.62 mcd (Hepp et al., 2006). Glacial-to-interglacial transitions are diffuse and characterized by a gradual change in physical and geochemical sediment parameters. Interglacial-to-glacial transitions are characterized by a sharp lithologic boundary. MSMZs are coupled to the glacial–interglacial cyclicity and consistently occur at glacial terminations (Hepp et al., 2006; Pudsey, 2002).

Magnetic susceptibility measurements of single samples containing hemipelagic sediment, silt layers or IRD (Fig. 3d), from above and below the MSMZ, clearly show that the magnetic susceptibility of samples with silt layers (solid circles; average 600 10^{-5} SI) is about three times higher than of samples without silt layers (open circles; average 200 10^{-5} SI). High total magnetic susceptibility is noticed in the lower part of the IRD dominated sections (between 104.30 and 103.66 mcd, Fig. 3c). The loss of magnetic susceptibility in the MSMZ is observed in samples with and samples without silt layers, independent of changes in grain-size (Fig. 3d, small arrows). Within the upper part of the MSMZ, coarse fraction samples (coarse sand and gravel) with lithic fragments from IRD preserved their singular magnetic signal (Fig. 3d, large arrow). Neither the lower nor the upper boundary of the MSMZ coincide with changes in silt layer occurrence or IRD supply in all grain-size fractions: (1) turbidity silt layers are continuous across the sharp onset of the MSMZ, (2) the recovery of the magnetic signal in the fine fraction marks the end of the MSMZ during the onset of an episode of massive IRD gravel supply. However, we conclude that mineral- and grain-size selective processes, largely independent from changes in the lithogenic influx, modified the magnetic susceptibility signal.

To understand the MSMZ in the context of the full glacial–interglacial cycle, we compared the magnetic susceptibility signal with lithological and geochemical changes in the sedimentary record. Based on a previous Pliocene study (Hepp et al., 2006) and new data (Fig. 3, Appendix A) the following four sedimentary units emerge:

(Unit 1) Graded silt layers (mode 30 μm) with an erosive base (Fig. 3a) are the carriers of the highest magnetic susceptibility signal (Fig. 3d, solid circles). IRD gravels are not present (Fig. 3b). The clay mineral composition is dominated by illite and elevated chlorite concentrations in Pliocene (Appendix B; Hillenbrand and Ehrmann, 2002) and Pleistocene and Holocene (Lucchi and Rebesco, 2007; Lucchi et al., 2002b) core sections. The amount of total organic carbon and sulfur is increased. This unit is interpreted as glacial. Grounded ice extended to the shelf edge and recurring turbidity events transported glacially eroded terrigenous material onto Drift 7 as graded silt layers (mode 30 μm) with an erosive base (Fig. 3a). High terrestrial fluxes increased the overall sedimentation rate and led to an improved total organic carbon burial efficiency (Fig. 3i). Comparable low biogenic barium records (Fig. 3k) in the glacial sequences reflect a terrigenous dominated sedimentation regime.

(Unit 2) The lower boundary of the MSMZ (105.38 mcd, Fig. 3c) is not accompanied by an abrupt lithological change. Silt layer frequency (Fig. 3a), sedimentation rate and Fe/Ti ratio (Fig. 3f, arrow) decrease gradually. Concurrently the opal accumulation increases of about 12% (Fig. 3h, arrow). This unit is interpreted to be deposited during deglaciation. During deglaciation the frequency of ice advances to the shelf edge decreased leading to a reduced terrigenous input. Expanded open sea conditions lead to an increase in primary bioproduction (Fig. 3h). Some minor lithological changes occur, as documented by gradual shifts in illite and chlorite concentration (Appendix B). A change in the paramagnetic mineral content is expressed by an increase in magnetic susceptibility of about 5 10^{-9} m^2/kg (Fig. 4). In contrast the sharp lower boundary of the MSMZ (105.38 mcd, Fig. 3c) is independent from the observed gradual glacial-to-interglacial lithological shifts (Appendix B) but accompanied by a prominent drop in the non-paramagnetic mineral concentrations, documented by a decrease in magnetic susceptibility of ~2 10^{-2} m^2/kg (Fig. 4).

(Unit 3) The end of the deglaciation is characterized by a cessation of turbidite events (Fig. 3a) and the simultaneous onset of massive IRD gravel input (Fig. 3b). This unit, in the following termed collapse of the regional ice sheet (ISC), represents the time when excessive ice of the preceding glacial rapidly melts down and the ice sheet retreats from the shelf. Coarse lithic fragments of the IRD (Fig. 3b) suppress the MSMZ characteristics in the uppermost part. The massive occurrence and good preservation indicate deposition from the water column without reworking, bottom transport or bioturbation. The top of the diatom ooze layer marks the upper boundary of the MSMZ in the fine fraction (Fig. 3d, open circles; Fig. 5a).

(Unit 4) High BSiO2 (Fig. 3h) and biogenic barium values (Fig. 3k), common IRD input (Fig. 3b) and the absence of silt layers (Fig. 3a) on the drift are interpreted as full interglacials with a retracted ice sheet that does not reach the shelf edge. Bioturbation and poor organic matter preservation reflect lower hemipelagic sedimentation rates. The clay mineral composition is dominated by illite and reduced chlorite concentrations (Appendix B). Paramagnetic mineral concentrations stay stable whereas non-paramagnetic mineral concentrations recover after the severe drop during deglaciation (Fig. 4). The re-advance of the grounded ice sheet at interglacial-to-glacial transitions re-initiates frequent turbidites associated with increased sedimentation rates, improved preservation of organic material and an abrupt cessation of IRD supply to the drift.

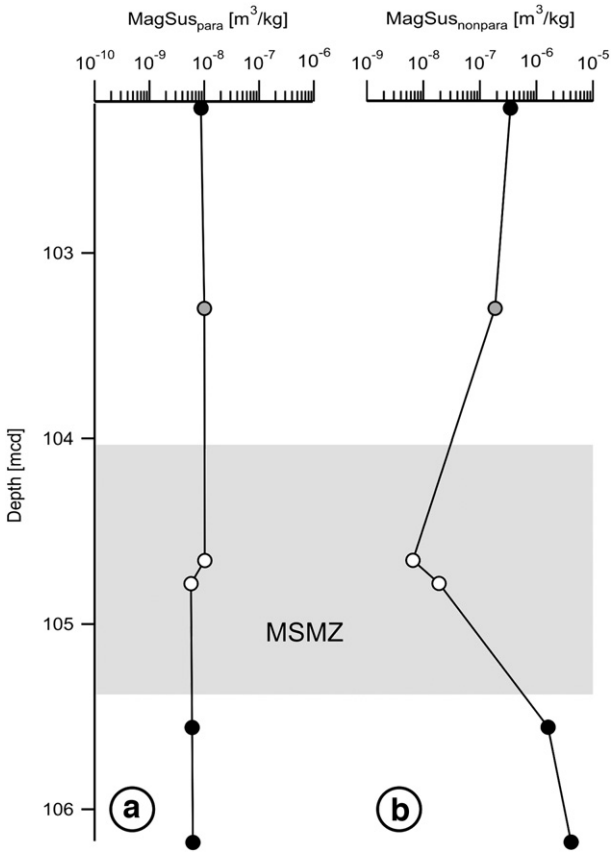

Fig. 4. The diagram shows the (a) paramagnetic and (b) non-paramagnetic magnetic susceptibility fraction deduced from magnetic hysteresis loops given in Appendix C. While paramagnetic susceptibility shows virtually no variation across the glacial–interglacial interval the non-paramagnetic susceptibility is significantly reduced during the MSMZ (Solid circles = samples from glacial intervals, grey circles = samples from interglacial interval, open circles = samples from MSMZ, shaded area).

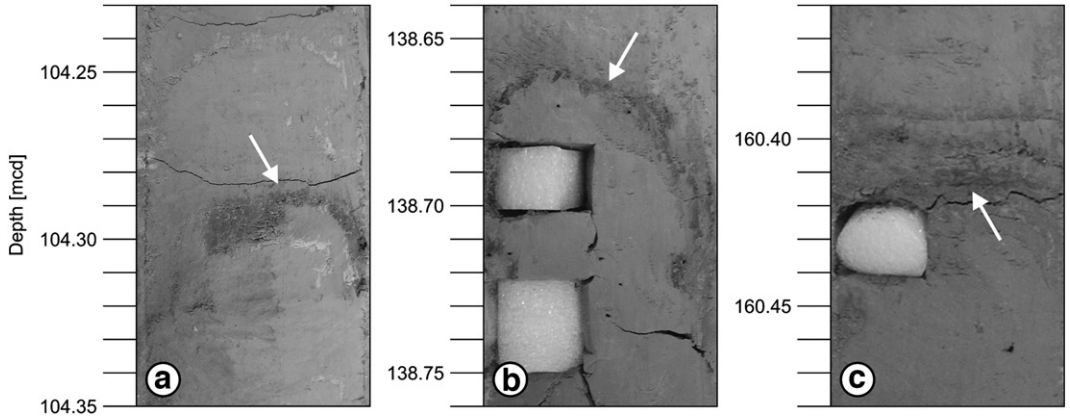

Fig. 5. Three examples for diatom ooze layers at the glacial–interglacial transition: (a) 104.30 mcd, (b) 138.67 mcd, and (c) 160.41 mcd. The diatom ooze layers occur above MSMZ and mark the end of deglaciation. The images give an impression about the appearance of the diatom ooze layers in the sediment core.

4.3. What caused the magnetic susceptibility minima zones?

To identify possible MSMZ triggers like dilution effects, changes in provenance or early diagenesis processes we analyzed magnetic susceptibility, clay mineral composition and organic fluxes across a glacial–interglacial transition.

The lower part of the MSMZ is associated with an increase in diamagnetic $BSiO_2$ (Fig. 3h, arrow) by a factor of 3 and a slight decrease in Fe/Ti ratio (Fig. 3f). Those changes are, however, insufficient to explain the abrupt drop in magnetic susceptibility by one order of magnitude. Dilution effects by diamagnetic and paramagnetic sediment compounds can be further ruled out since high opal contents continue across the upper boundary of the MSMZ. The independence of MSMZ from sedimentary dilution effects is further confirmed by the Fe/κ ratio (Fig. 3g) introduced by Funk et al. (2004a,b). Increased Fe/k ratios highlight sediment intervals which have been affected by early diagenetic iron/magnetite reduction producing distinct losses in magnetic susceptibility while the total concentration of solid-phase iron stays constant. Signs of a possible diagenetic imprint are further seen in strong enrichments of redox sensitive elements like iron and manganese in the upper part of the MSMZ (Fig. 3e,f, large peaks at 104.30 mcd, Appendix A) and in the asynchrony of biogenic barium and $BSiO_2$ rise (Fig. 3k, arrow). Diatom concentrations and biogenic barium are commonly synchronous in Holocene and Pleistocene sections that lack MSMZs (Hillenbrand and Fütterer, 2002; Pudsey, 2000).

Low-temperature magnetic measurements and high-field magnetic hysteresis loops on samples across a glacial cycle were performed to detect the type of magnetic mineral species and possible provenance changes. All samples show a drop in remanence intensity at temperatures ranging from 114 to 122 K (Appendix C) indicating the presence of nearly stoichiometric magnetite. Magnetite with cubic symmetry at room temperature shows a change to monoclinic symmetry below a temperature of 120 K. This phase transition is accompanied by higher remanent magnetizations towards lower temperatures. Deduced from these FC measurements, there is no indication for other remanence carrying minerals, e.g. monoclinic ferrimagnetic pyrrhotite (Fe_7S_8), characterized by a low-temperature transition at 34 K. Also no evidence for the presence of hematite (Fe_2O_3) was found. Hematite undergoes a discontinuity in magnetic properties at around −15 °C showing higher remanences above this temperature (Liebermann and Banerjee, 1971). Greigite (Fe_3S_4), however, does not exhibit a phase transition in the mentioned temperature range and thus measurements of the magnetic hysteresis at room temperature and peak field strengths of 7 T were carried out.

Data from low-temperature demagnetization of a remanence acquired at 5 K after cooling in a 5 T magnetic field (FC) across one glacial–interglacial cycle show a dramatically reduced relative amount of almost non-stoichiometric magnetite of stable single domain grain-size in the MSMZ (Appendix C). Our measurements prove that magnetite of variable grain-size is present in all samples investigated without evidence for significant amounts of other magnetic minerals.

Zero-field heating of a remanence acquired at 5 K after cooling in a 5 T magnetic field after zero-field cooling (ZFC) and FC showed that in samples from glacial and interglacial intervals below and above the MSMZ (106.177, 105.557, 103.3 and 102.22 mcd), the FC curves are lower than the respective ZFC curves (Appendix C). This was observed for several natural and synthetic magnetite samples and seems to be typical of multidomain magnetite larger than ~10–14 µm (Brachfeld et al., 2002b). In contrast, samples from the MSMZ (104.782 and 104.657 mcd) demonstrate higher FC than ZFC curves pointing to magnetite particles of smaller average grain-sizes. This supports the results of the hysteresis measurements (Appendix C) giving higher remanence to saturation magnetization (M_{RS}/M_S) ratios of ~0.12 and coercive field (H_C) values for the MSMZ samples, again indicating smaller grain sizes (Day et al., 1977). In general, magnetic hysterisis loops provide no evidence for the presence of greigite. High M_{RS}/M_S ratios of ~0.5 are typical for greigite (Roberts, 1995) in contrast to the much lower ratios determined in the present study.

The MSMZ lost most of its magnetite (up to 99% of the non-paramagnetic susceptibility, Appendix C) in all grain-size ranges. However, some (normally less resistant) small particles in the MSMZ must have been protected from reductive dissolution. Plausible mechanisms for protection are the inclusion of small magnetite particles within lithic fragments (Talarico et al., 2003) or within volcanic glass (Heider et al., 1993) or cloudy feldspar (Hounslow and Maher, 1995).

In addition to the findings from magnetic analysis we found no significant change in clay mineral composition (Appendix B). In general, illite dominates, whereas smectite and kaolinite are insignificant and below 10 wt.%. Corresponding to findings by Hillenbrand and Ehrmann (2002) the chlorite concentration is enhanced in glacials. Small variations in clay mineral concentration in the middle of the MSMZ are unrelated to the lower and upper boundary of the MSMZ.

In summary, the FC, ZFC, hysteresis measurements and clay mineral measurements demonstrate that the reduced signal of magnetic susceptibility is related to the decreased concentration of magnetominerals rather than to a dilution effect or a change in provenance of the source material causing significant changes in the magnetic or clay mineral assemblage. The decreased overall magnetic susceptibility in the MSMZ between 105.38 and 104.44 mcd (Fig. 3) is best explained by an early diagenetic process of sufficient strength and duration to dissolve small as well as large magnetite grains.

Early diagenetic processes affect the preservation of primary signals and the interpretation of proxies in sediments. After their deposition marine sediments are subject to a variety of geochemical and microbiological processes. The re-mineralization of sedimentary organic matter plays a key role in many of these processes. Degradation of organic matter at suboxic, sulfidic or methanic levels is accompanied by a gradual dissolution of primary ferro-magnetic iron minerals. This gradual, mineral- and grain-size selective process makes rock magnetic parameters, particularly those related to concentration (e.g. magnetic susceptibility), a sensitive measure for diagenetic intensity (Funk et al., 2004a,b). The degree of demagnetization is proportional to the amount of mineralized organic material (Funk et al., 2004a). Many examples of iron reduction events induced by the degradation of organic matter have been discussed in the study of Funk et al. (2004b) as part of their examination of Pleistocene equatorial Atlantic sediment cores. Increased glacial organic carbon fluxes led to similar losses in the magnetic susceptibilty signal. Diagenetic redistributions of redox-sensitive elements in otherwise well-ventilated open oceanic conditions are also known from organic-rich turbidite deposits in the Madeira abyssal plain (Thomson et al., 1998).

4.4. Pliocene magnetic susceptibility minima zones versus Pleistocene–Holocene magnetic anomalies

Studies on late Pleistocene–Holocene sedimentary sequences of Drift 7 suggest scenarios of glacial environmental conditions with an absence of bioturbation, general low organic carbon content (Lucchi and Rebesco, 2007; Sagnotti et al., 2001) and repeated sediment magnetic anomalies (Sagnotti et al., 2001). Those scenarios seem to oppose our early Pliocene scenario based on the diagenetic alteration of the magnetic susceptibility signal in response to high paleoproductivity.

The comparison of SEDANO cores (Sagnotti et al., 2001) and late Pleistocene core sections of ODP Site 1095 (Appendix A) with our analyzed Pliocene intervals suggests fundamental differences in the degree of the diminishment of magnetic susceptibility and the occurrence of intermittent magnetic mineral phases. The Pleistocene and Holocene magnetic susceptibility record at ODP Site 1095 (Appendix A) shows no significant reductions related to glacial and interglacial transitions. The early Pliocene MSMZs occur only during the deglaciation, whereas the Pleistocene magnetic anomalies presented by Sagnotti et al. (2001) occur through the entire marine isotope stages (MIS) 7 to 2). Magnetite is the dominant carrier of the Pliocene magnetic susceptibility signal (Appendix C) and overall high organic fluxes prevented the preservation of pyrrhotite. In contrast, Sagnotti et al. (2001) found indications for the presence of greigite or pyrrhotite in late Pleistocene Drift 7 sediments. The proposed glacial, sea ice dominated scenarios of Sagnotti et al. (2001) and Lucchi and Rebesco (2007) point to different diagenetic processes coupled to different environmental scenarios, which are not applicable for the early Pliocene drift setting.

Florindo et al. (2003) presented another possible reason for magnetic susceptibility losses. They proposed that magnetite is unstable under conditions of elevated dissolved silica concentrations and predict that magnetite will be dissolved to produce iron-bearing smectite. In Pliocene core sections of ODP Site 1095 the dissolved silica concentration corresponds to the opal concentration in the sediment (Fig. 7d), which is not elevated during MSMZ only (Fig. 3h). On the other hand in the MSMZs, analysed in this study, we did not found indications for a significant enhancement of smectite formation (Appendix B). This is not surprising due to the low magnetite contents.

However, the analyzed glacially triggered Pliocene MSMZs are strongly linked to short-term changes in organic matter fluxes, which likely prevent the establishment of equilibrium conditions. Other aspects regarding the upper boundary of the MSMZ are addressed in the following scenario that attempts to bind the suggested succession of diagenetic processes into a refined conceptual model integrating oceanographic-cryospheric and sedimentologic aspects.

4.5. Early Pliocene boundary conditions required to produce MSMZ

Diagenesis driven by organic carbon re-mineralization is a complex function of organic matter quality and quantity, sedimentation rate, intensity of bioturbation, ocean ventilation and deepwater oxygen content. The Southern Ocean biological pump and coupled opal and organic carbon deposition are bound to winds, ocean circulation and sea ice (Anderson et al., 2002). Late Miocene to early late Pliocene warm climate conditions and a reduction of 22% in sea ice cover at the continental rise, relative to modern conditions, are generally accepted for Antarctica (Anderson et al., 2002; Hillenbrand and Fütterer, 2002; Whitehead et al., 2005). Global ice volume records by Lear et al. (2000) indicate a strong reduction in overall ice volume for this time interval. Despite an overall ice volume reduction, the late Miocene to early late Pliocene ice dynamics increased with frequent advances of the inland ice sheet to the shelf edge (Barker and Camerlenghi, 2002).

We speculate that at the end of the deglaciation (Fig. 6), during times of rapid shelf ice sheet break down, an increased freshwater discharge, a stratified water column and fertilization of the ocean by terrigenous and dust-bound iron could have enhanced export productivity (Abelmann et al., 2006; Kumar et al., 1995) under sea ice free conditions. Moreover, stratification, nearly stagnant deepwater conditions and the absence of bioturbation are possible causes for the preservation of current sensitive diatom oozes on the flank of an elevated topographic feature like Drift 7. High organic carbon export rates and reduced bottom water ventilation during the break down of the shelf ice sheet provided the framework for the development of suboxic conditions in surface sediments and most likely even for sulfate reduction ocurring close to the sediment water interface (Fig. 6).

However, we propose that freshwater pulses as a consequence of partial collapse of the APIS initiated massive short-term diatom blooms above the continental rise leading to the deposition of diatom ooze layers on the sea floor. The diatom ooze drape sealed off the underlying sediments (Fig. 6) resulting in the initiation of suboxic conditions.

4.6. Long-time record of redox events

Diagenetic processes altering magnetic susceptibility signals in ODP Site 1095 sediments are found to act on long and short time-scales with changing intensities and frequencies of recurrence. For the period from 8.49 to 3.17 Ma, sixty-four MSMZs were identified (Figs. 2, 7a). Our repeated MSMZs are linked to short-term changes over glacial-interglacial time scale. All zones show similar patterns in demagnetization, shape and magnitude in the magnetic susceptibility signal, and they are in certain cases accompanied by diatom ooze layers. Twelve diatom ooze layers between ~7.7 and 3.8 Ma are clearly related to MSMZs.

On long time-scales we have to consider that the sulfate-methane-transition zone which is currently located between 157.97 and 158.50 mcd (SMT; Fig. 7) could have influenced some of the MSMZs. The remarkable depth extension of the MSMZ at this depth may be explained by the long-term fixation of the present SMT (Fig. 7b). This fixation requires equilibrium conditions between downward sulfate flux and upward methane flux (e.g. Riedinger et al., 2005) and is expressed in a linear sulfate profile (ODP Leg 178 Shipboard Scientific Party, 1999).

The de-compacted MSMZ interval length in meter is plotted against age (Fig. 7b). The spatial extent of a MSMZ can be related

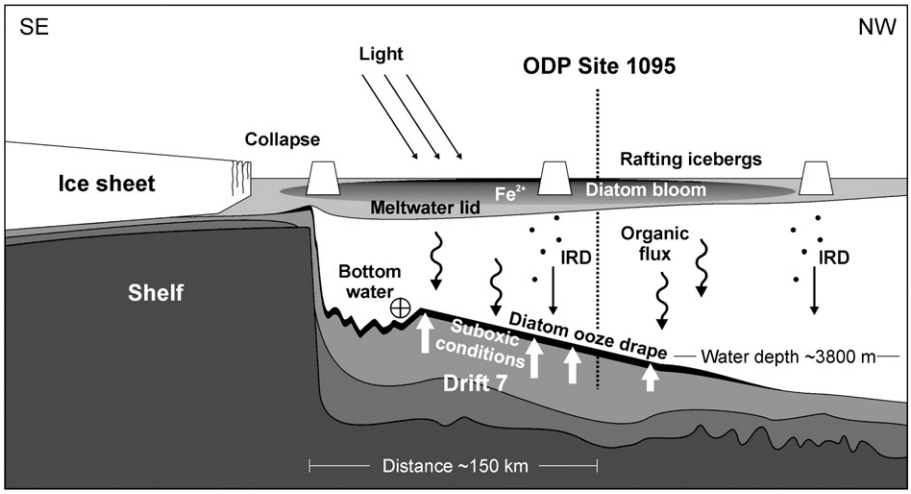

Fig. 6. During intense ice sheet collapse, the retreating ice sheet and a large meltwater lid leads to increased iron fertilization, a short-term diatom bloom and the stratification water column. Reduced bottom water ventilation and high export productivity foster the preservation a diatom ooze drape on the drift resulting in periodic suboxic conditions in surface sediments.

either to the duration or the intensity of the phase of reduced magnetic susceptibility, indirectly controlled by the amount of organic matter input. Comparable trends in this parameter and the diagenesis intensity proxy of Funk (2004a; Fig. 7c), however, indicate that strong demagnetization events commonly have a larger diagenesis penetration depth. Both parameters show some similarities with the export productivity proxy $BSiO_2$ (Fig. 7d) and the relic preservation of total organic carbon (TOC; Fig. 7e). The similarities suggest that intensity and duration of diagenesis are subject to the organic input.

During the Pliocene warming phase the indicators for intensity and duration of diagenesis, for biogenic input ($BSiO_2$) and for preservation of organic matter in the sediment (TOC) increase to maximum values (between 190.0 and 46.0 mcd; 5.6–2.7 Ma). Following this 3 Ma period of exceptionally high productivity, the late Pliocene saw a gradual decrease of biogenic silica deposition south of the APF. This is observed in a multitude of sediment records in the Atlantic and Pacific sector of Southern Ocean and has been used to document the northward shift of the APF between 3.3 and 2.3 Ma (Hillenbrand and Cortese, 2006). Synchronous with the decrease of biogenic silica deposition characteristic MSMZs cease at 79.35 mcd (~3.17 Ma). This reflects the global cooling trend coupled to the Northern hemisphere glaciation and the growth of the Antarctic ice sheets.

The global cooling resulted in a reduction of Antarctic ice sheet dynamics, decreased terrigenous sediment input, a seaward spread of sea ice and less pronounced ISCs during Antarctic deglaciations. At 3.17 Ma, organic export productivity and sedimentation rates fell below a threshold level, preventing sulfate reduction to occur at significant rates in subsurface sediments (Figs. 2, 7). Our assumption

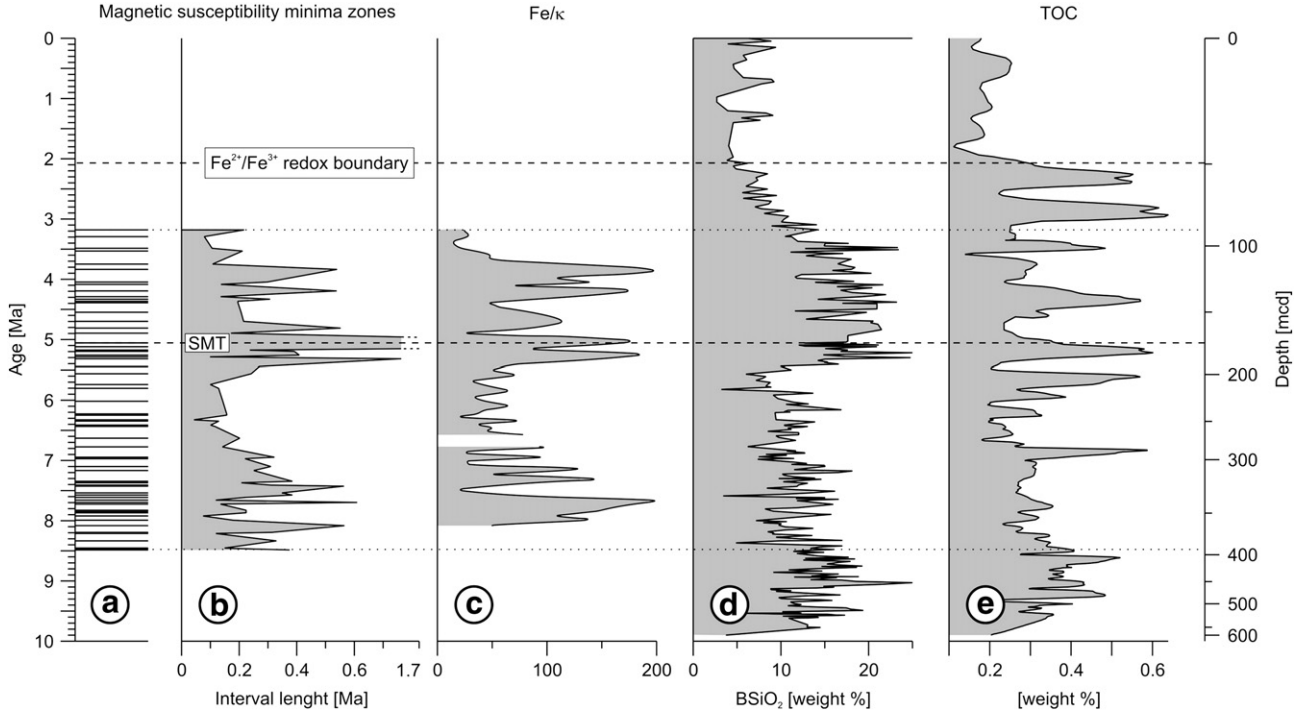

Fig. 7. MSMZs from ODP Site 1095A and B. The 'bar code' and the dotted lines represent the occurrence and range of (a) MSMZs. The dashed lines represent the modern positions of Fe^{2+}/Fe^{3+}-redox boundary and the sulfate–methane-transition (SMT), respectively. Curves represent (b) the de-compacted interval length of MSMZs as a parameter related to the relative duration or extent of penetration of the diagenesis event, (c) the Fe/κ ratio as an indicator for the intensity of diagenesis, (d) biogenic silica (opal) as proxy for palaeoproductivity, and (e) total organic carbon as proxy for organic preservation. Core lengths were de-compacted on primary length using factor of porosity. Curves of Fe/κ ratio and total organic carbon were smoothed using moving average and Hilbert transformations.

of a change in the sedimentary regime that followed the transition of the Antarctic ice regime contributes to the recent discussion about a continent-wide change in basal ice conditions about 3 Ma (Rebesco et al., 2006, see also comment by R. D. Larter, doi:10.1130/G23422C.1, and reply, doi:10.1130/G23894Y.1; Rebesco and Camerlenghi, 2008).

We speculate that after 3.17 Ma a more vigorous deglacial Antarctic Bottom Water (AABW) formation resulted in an enhanced deepwater ventilation and oxygenation, with an overall reduced organic carbon flux to the seafloor (and/or a reduced preservation) preventing the development of lasting diatom oozes and temporary oxygen-reduced conditions.

5. Conclusion

In this study we present a unique late Miocene–early Pliocene record of sixty-four zones with prominent losses in the magnetic susceptibility signal (MSMZ). The MSMZs were identified in the magnetic susceptibility signal of ODP Site 1095 cores, taken on a sediment drift on the Pacific continental rise of the Antarctic Peninsula. The MSMZs, expressed as phases of diminished magnetic susceptibility, are comparable in their shape and magnitude and occur commonly at glacial-to-interglacial transitions.

With detailed analyzes of organic matter, magnetic and clay mineral compositions we could show that, during early Pliocene times (and perhaps back to the late Miocene), exceptionally high organic matter fluxes in combination with weak bottom water currents produced temporary oxygen-depleted/suboxic conditions in the uppermost sediments. Other processes like dilution effects or changes in source and provenance of the sediments are insufficient to produce the MSMZs.

The findings for the Pliocene deposits differs clearly from scenarios proposed for late Pleistocene–Holocene sedimentary sequences of Drift 7 (Lucchi and Rebesco, 2007; Sagnotti et al., 2001), where repeated sediment magnetic anomalies occur under glacial environmental conditions. During these times low organic fluxes control the mixture of magnetite and pyrrhotite.

On long time-scales the MSMZ record reflects major trends in globally paleoceanographic and climatic change and the consequent variability in primary export production. The early Pliocene was a time of global enhanced bioproductivity. Following the Antarctic ice sheet stabilization, between 3.3 and 2.3 Ma, the flux of organic matter and sedimentation rates fell below a threshold level preventing the development of more extensive reducing conditions in near surface sediments.

Drift 7 is part of the Southern Ocean, which ventilates a large fraction of the World Ocean, today. It is remarkable that changes in paleoceanographic boundary conditions could result in temporary suboxica in open ocean's near surface drift sediments contributing to a better preservation of magnetite during this period.

Acknowledgement

Samples were provided by Ocean Drilling Program (ODP). We thank the Bremen Core Repository (BCR) team for their kind support. Thanks to Jens Grützner and Ursula Röhl at Bremen University who provided XRF data. Some $BSiO_2$ data from single samples were part of a bachelor thesis by Sophie Fath prepared in our working group. In this regard the help of Gerhard Kuhn and Rita Froehlking (Alfred Wegener Institute for Polar and Marine Research, AWI, Bremerhaven) during the measurements is greatly acknowledged. We thank Ismene Seeberg-Elverfeldt at Bremen University for her expertise on diatoms. Fruitful discussions with Syee Weldeab (Leibniz Institute of Marine Sciences, IFM-GEOMAR, Kiel) improved our understanding of water mass stratification. We are grateful to Gerald Dickens (Rice University, Houston TX) for his constructive comments on an earlier version of the manuscript. We thank Angelo Camerlenghi and Claus-Dieter Hillenbrand for their comments and suggestions that improved our manuscript. This research was funded by the Deutsche Forschungsgemeinschaft (DFG projects MO1059/1 and HE5377/1) and by the MARUM-Center for Marine Environmental Sciences, University of Bremen.

Appendix A

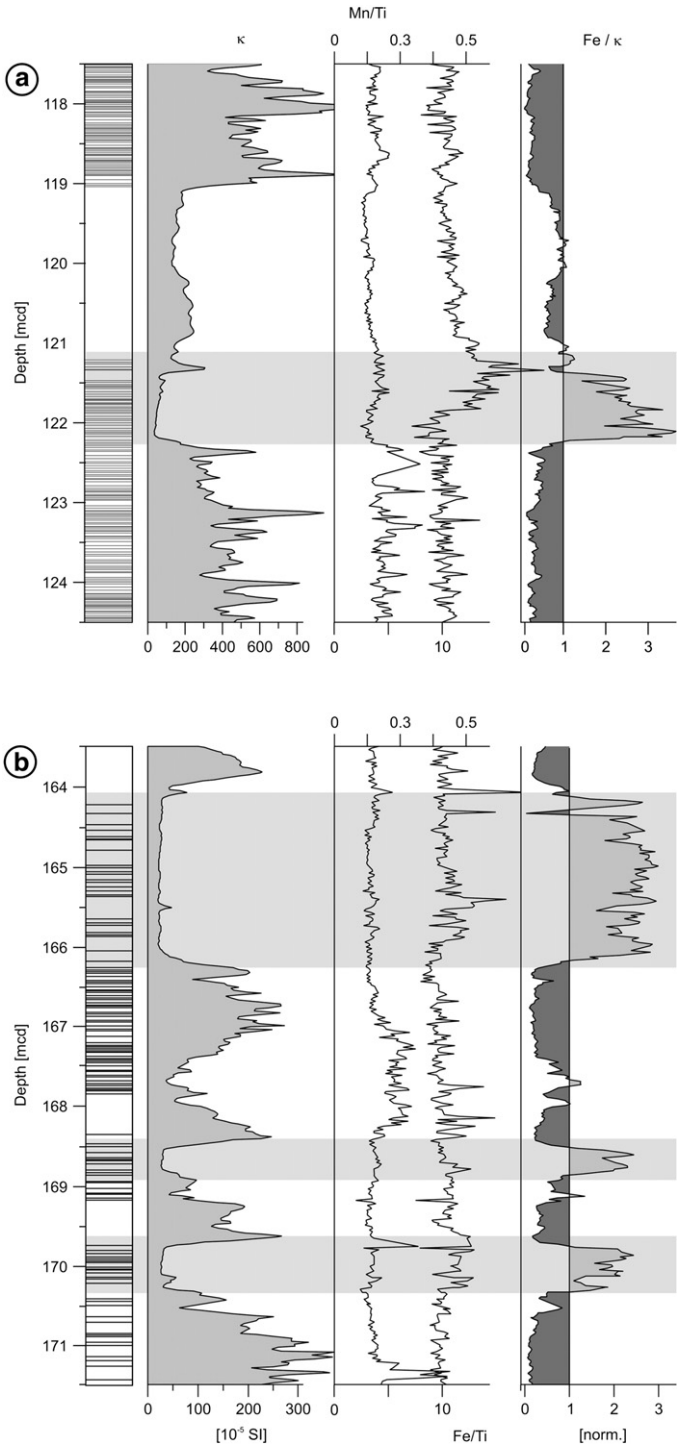

Fig. 8. Examples of MSMZ in the context of complete glacial–interglacial cycle (a) 124.50–117.50 mcd and (b) 171.50–163.50 mcd: absolute position of silt layers, magnetic susceptibility (κ) from shipboard logging data, Mn/Ti ratio and Fe/Ti ratio from X-ray fluorescence spectrometry (XRF) logging and normalized Fe/κ ratio (Shaded area = MSMZ). A prominent Mn-peak is not expressed for each core section.

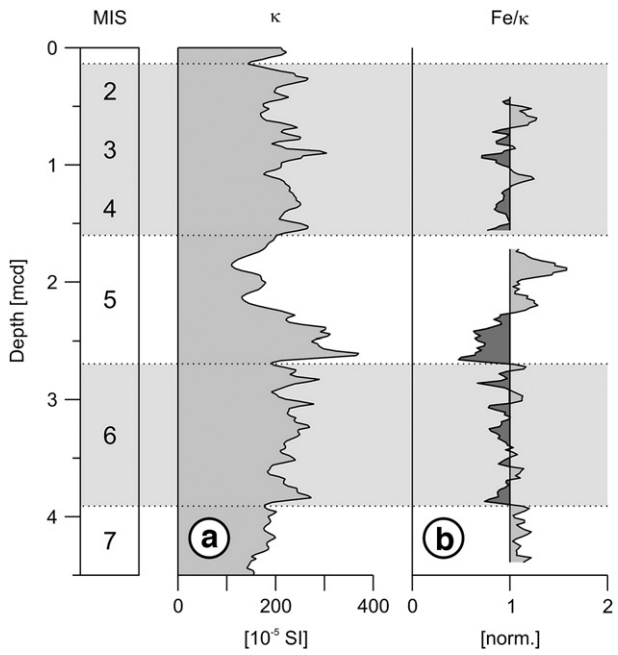

Fig. 9. Magnetic susceptibility data (κ) and normalized Fe/κ ratio of upper Pleistocene to Holocene core sections of ODP Site 1095. We adopted marine isotope stages (MIS) given in Lucchi et al. (2002a,b) by comparing SED-15 with ODP Site 1095 magnetic susceptibility data.

Appendix B

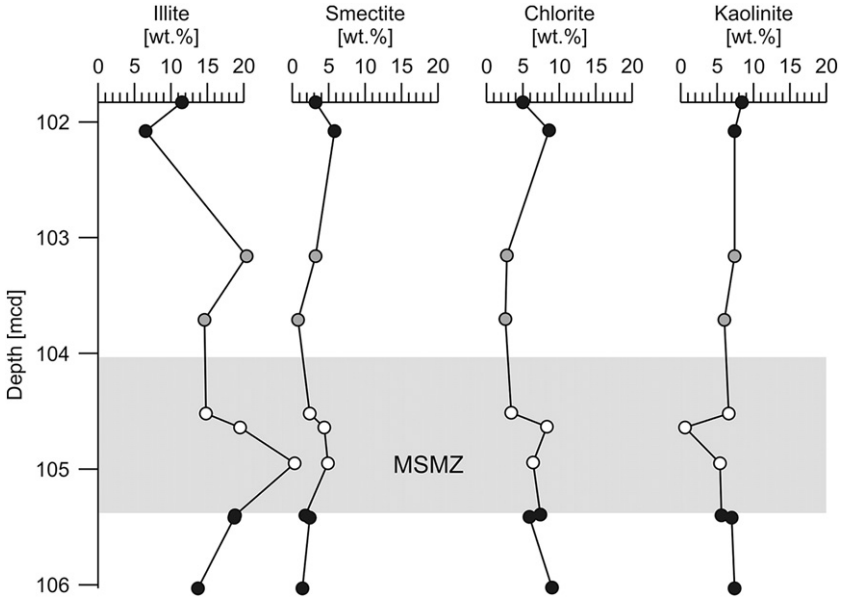

Fig. 10. Absolute clay mineral concentration across a glacial–interglacial interval (107.5–101.5 mcd). Illite dominates in all lithologic units. Small variations in the clay mineral compositions, e.g. in the middle of the MSMZ (shaded area), are not related to the onset and termination of the MSMZ (Solid circles = samples from glacial intervals, grey circles = samples from interglacial interval, open circles = samples from MSMZ). In contrast to previous studies by Hillenbrand and Ehrmann (2002) and Lucchi et al. (2002a,b), we quantified the full-pattern of mineral phases. The derived absolute clay mineral concentrations are of high precision (Vogt et al., 2002), but not directly comparable to relative clay mineral percentages by means of empirical factors (Biscaye, 1965).

Appendix C

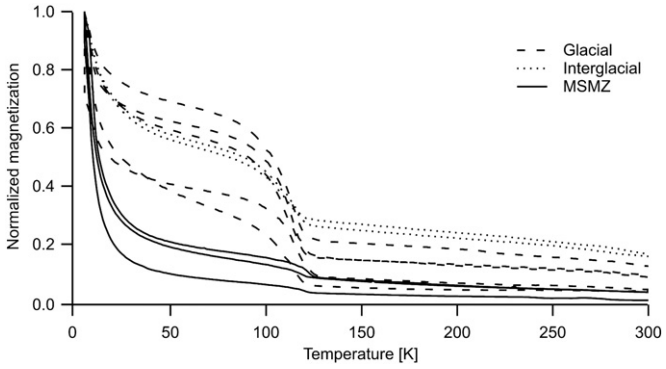

Fig. 11. Low-temperature demagnetization of a remanence acquired at 5 K after cooling in a 5 T magnetic field. All samples from glacial and interglacial intervals (106.177, 105.557, 103.3 and 102.22 mcd) and MSMZ (104.782 and 104.657 mcd) show a drop in remanence intensity at temperatures ranging from 114 to 122 K indicating the presence of nearly stoichiometric magnetite. The normalized magnetization during MSMZ glacial–interglacial interval is remarkable low, indicating reduced magnetite concentrations.

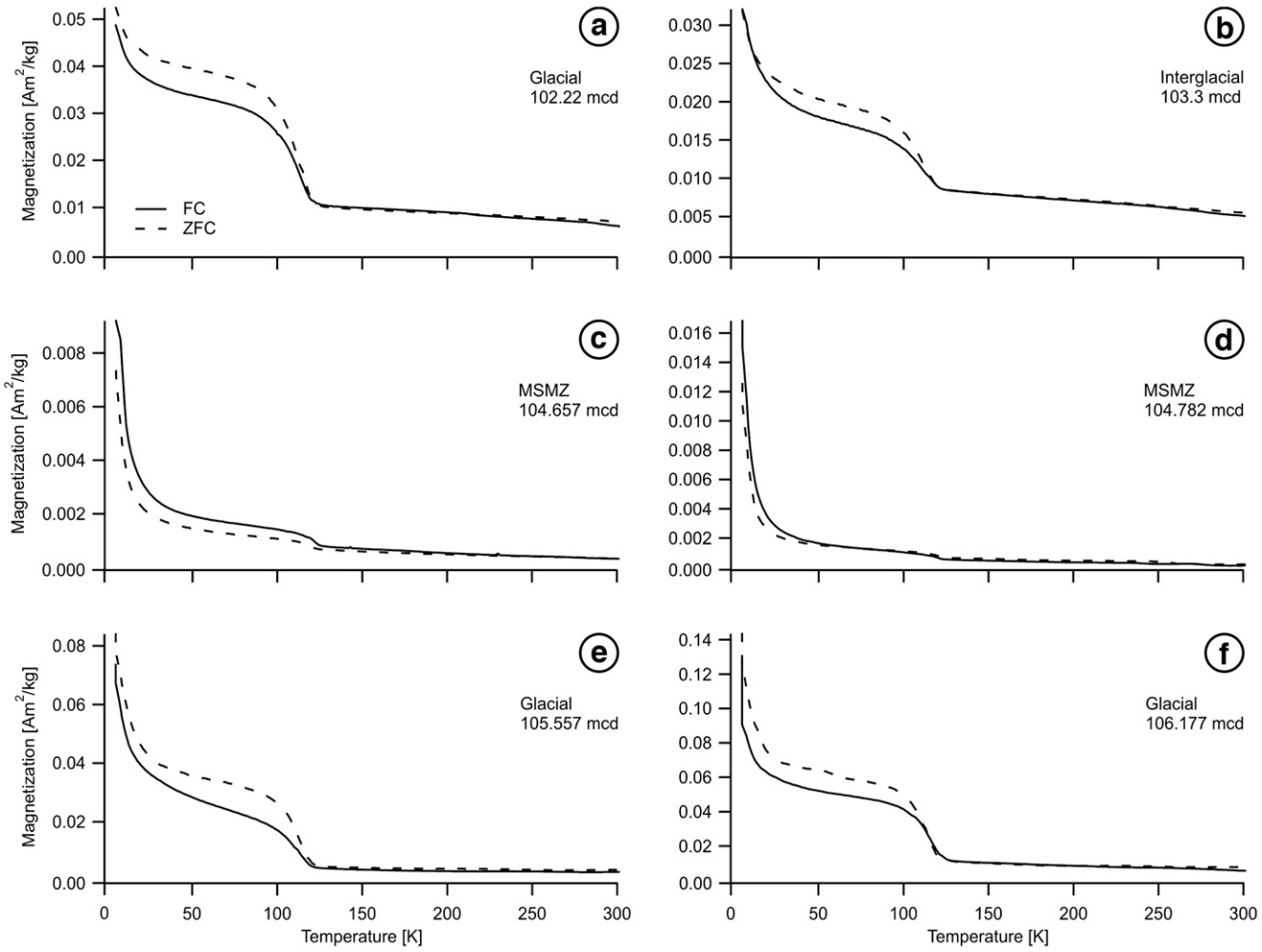

Fig. 12. Low-temperature demagnetization of a remanence acquired in a magnetic field of 5 T at a temperature of 5 K after cooling the samples in zero-field (ZFC, dotted line) and in presence of a 5 T magnetic field (FC, solid line). The ZFC curves for samples from glacial and interglacial intervals (106.177, 105.557, 103.3 and 102.22 mcd) are higher than the respective FC curves. In contrast the ZFC curves from the MSMZ (104.782 and 104.657 mcd) are lower than FC curves pointing to magnetite particles of smaller average grain-sizes. These results may appear surprising in context with the postulated diagenetic dissolution, which in particular affects small particles due to their high surface-to-volume ratio. Beyond, stoichiometric magnetite is most heavily affected by diagenetic dissolution (Garming et al., 2005). The following scenario may explain this issue: We assume an input of nearly constant composition with respect to the para- and ferrimagnetic constituents during both glacial and interglacial times, since our measurements prove that magnetite of variable grain-size is present in all samples investigated without evidence for significant amounts of other magnetic minerals. Changes in the paramagnetic fraction, large enough to explain the drastic changes in the magnetic susceptibility record, are not likely since only the non-paramagnetic magnetic susceptibility shows distinctly reduced values within the MSMZ whereas paramagnetic susceptibility (as calculated from the linear slope of the hysteresis loops at high magnetic fields) exhibits only very minor variations (Fig. 4). Thus, the decreased overall magnetic susceptibility is basically caused by a diagenetic potential within the MSMZ sufficient to dissolve small as well as large magnetite grains. The remaining (normally less resistant) small particles in the MSMZ must have been protected from dissolution.

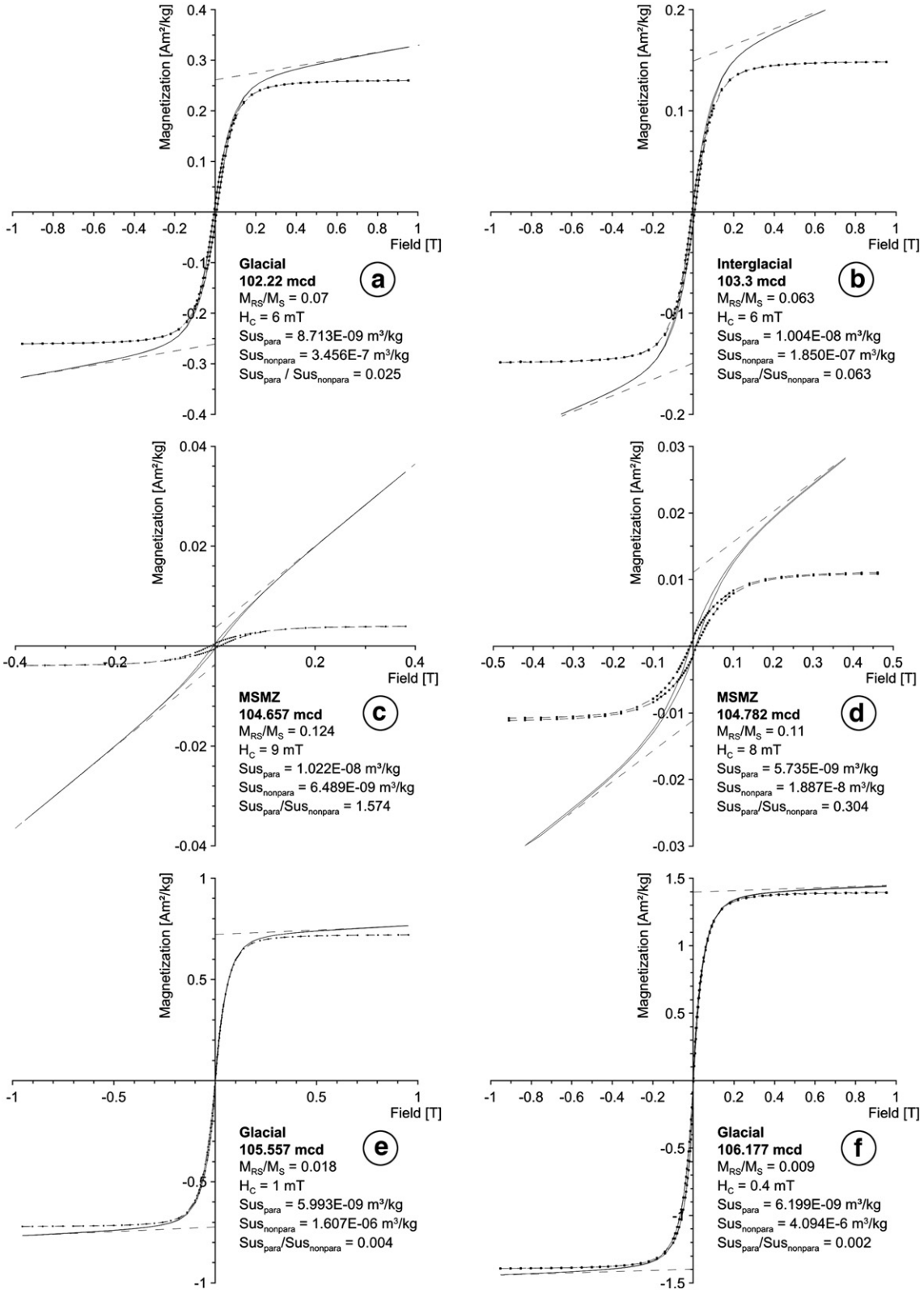

Fig. 13. Magnetic hysteresis loop of samples in a peak field of 7 T. For the sake of clarity only the interval from −1 to +1 T field is plotted here. Solid line indicates the original loop; dashed line with dots represents the same data corrected for the linear contribution (dashed lines) of paramagnetic susceptibility. A typical property of greigite is its high ratio of M_{RS}/M_S at about 0.5 or even higher whereas mixtures of natural magnetite demonstrate values ranging from 0.1 to 0.25 as, e.g., Sagnotti et al. (2001) had found for Late Pleistocene Drift 7 sediments. The results of six samples lie between 0.01 and 0.12 representing magnetite particles of pseudo-single-domain to multi-domain grain size with no indication for the presence of greigite.

References

Abelmann, A., Gersonde, R.E., Cortese, G., Kuhn, G., Smetacek, V., 2006. Extensive phytoplankton blooms in the Atlantic sector of the glacial Southern Ocean. Paleoceanogr. 21 (PA1013).

Acton, G.D., Guyodo, Y., Brachfeld, S.A., 2002. Magnetostratigraphy of sediment drifts on the continental rise of West Antarctica (ODP Leg 178, Sites 1095, 1096, and 1101). In: Barker, P.F., Camerlenghi, A., Acton, G.D., Ramsay, A.T.S. (Eds.), Proc. ODP Sci. Res. Texas A&M University, College Station, TX, pp. 1–61. [CD-ROM].

Anderson, R.F., Chase, Z., Fleisher, M.Q., Sachs, J., 2002. The Southern Ocean's biological pump during the Last Glacial Maximum. Deep-Sea Res. II 49 (9–10), 1909–1938.

Azizi, F., 2000. Applied Analyses in Geotechnics. E & FN Spon, New York. London, 254 pp.

Barker, P.F., 2002. Composite depths and spliced sections for Leg 178 Sites 1095 and 1096, Antarctic Peninsula continental rise. In: Barker, P.F., Camerlenghi, A., Acton, G.D., Ramsay, A.T.S. (Eds.), Proc. ODP Sci. Res. Texas A&M University, College Station, TX, pp. 1–15. [CD-ROM].

Barker, P.F., Camerlenghi, A., 2002. Glacial history of the Antarctic Peninsula from Pacific margin sediments. In: Barker, P.F., Camerlenghi, A., Acton, G.D., Ramsay, A.T.S. (Eds.), Proc. ODP Sci. Res. Texas A&M University, College Station, TX, pp. 1–40. [CD-ROM].

Biscaye, P.E., 1965. Mineralogy and sedimentation of recent deep-sea clay in the Atlantic Ocean and adjacent seas and oceans. Geol. Soc. Am. Bull. 76 (7), 803–832.

Brachfeld, S.A., Banerjee, S.K., Guyodo, Y., Acton, G.D., 2002a. A 13,200 year history of century- to millennial-scale paleoenvironmental change magnetically recorded in the Palmer Deep, western Antarctic Peninsula. Earth Planet. Sci. Lett. 194, 311–326.

Brachfeld, S.A., Guyodo, Y., Acton, G.D., 2002b. The magnetic mineral assemblage of hemipelagic drifts, ODP Site 1096. In: Barker, P.F., Camerlenghi, A., Acton, G.D., Ramsay, A.T.S. (Eds.), Proc. ODP Sci. Res. Texas A&M University, College Station, TX, pp. 1–12. [CD-ROM].

Cortese, G., Gersonde, R., Hillenbrand, C.-D., Kuhn, G., 2004. Opal sedimentation shifts in the World Ocean over the last 15 Myr. Earth Planet. Sci. Lett. 224 (3–4), 509–527.

Day, R., Fuller, M., Schmidt, V.A., 1977. Hysteresis properties of titanomagnetites: grain-size and compositional dependence. Phys. Earth Planet. Interiors 13, 260–267.

Dickens, G.R., Owen, R.M., 1996. Sediment geochemical evidence for an early–middle Gilbert (Early Pliocene) productivity peak in the North Pacific Red Clay Province. Mar. Micropaleontol. 27 (1–4), 107–120.

Dickens, G.R., Owen, R.M., 1999. The Latest Miocene–Early Pliocene biogenic bloom: a revised Indian Ocean perspective. Mar. Geol. 161 (1), 75–91.

Diekmann, B., et al., 2000. Terrigenous sediment supply in the Scotia Sea (Southern Ocean): response to Late Quaternary ice dynamics in Patagonia and on the Antarctic Peninsula. Palaeogeogr., Palaeoclimatol., Palaeoecol. 162 (3–4), 357–387.

Diester-Haass, L., Billups, K., Emeis, K.-C., 2005. In search of the late Miocene–early Pliocene "biogenic bloom" in the Atlantic Ocean (Ocean Drilling Program Sites 982, 925, and 1088). Paleoceanogr. 20. doi:10.1029/2005PA001139.

Dymond, J., Suess, E., Lyle, M., 1992. Barium in deep-sea sediment: a geochemical proxy for paleoproductivity. Paleoceanogr. 7, 163–181.

Farrell, J.W., et al., 1995. Late Neogene sedimentation patterns in the eastern equatorial Pacific ocean. In: Pisias, N.G., Mayer, L.A., Janecek, T.R., Palmer-Julson, A., van Andel, T.H. (Eds.), Proc. ODP Sci. Res. Texas A&M University, College Station, TX, pp. 717–756.

Florindo, F., Roberts, A.P., Palmer, M.R., 2003. Magnetite dissolution in siliceous sediments. Geochem., Geophys., Geosyst. 4 (7), 1053. doi:10.1029/2003GC000516.

Funk, J.A., von Dobeneck, T., Reitz, A., 2004a. Integrated rock magnetic and geochemical quantification of redoxomorphic iron mineral diagenesis in Late Quaternary sediments from the equatorial Atlantic. In: Wefer, G., Mulitza, S., Ratmeyer, V. (Eds.), The South Atlantic in the Late Quaternary: Reconstruction of Material Budgets and Current Systems. Springer, New York, pp. 237–260. Berlin, Heidelberg.

Funk, J.A., von Dobeneck, T., Wagner, T., Kasten, S., 2004b. Late Quaternary sedimentation and early diagenesis in the equatorial Atlantic Ocean: patterns, trends and processes deduced from rock magnetic and geochemical records. In: Wefer, G., Mulitza, S., Ratmeyer, V. (Eds.), The South Atlantic in the Late Quaternary. Reconstruction of material budgets and current systems. Springer, Berlin, Heidelberg, New York, pp. 461–497.

Garming, J.F.L., Bleil, U., Riedinger, N., 2005. Alteration of magnetic mineralogy at the sulfate–methane transition: analysis of sediments from the Argentine continental slope. Phys. Earth Planet. Interiors 151 (3–4), 290–308.

Haug, G.H., Tiedemann, R., 1998. Effect of the formation of the Isthmus of Panama on Atlantic Ocean thermohaline circulation. Nature 393 (6686), 673–676.

Heider, F., Körner, U., Bitschene, P., 1993. Volcanic ash particles as carriers of remanent magnetization in deep-sea sediments from the Kerguelen Plateau. Earth Planet. Sci. Lett. 118, 121–134.

Hensen, C., et al., 2003. Control of sulfate pore-water profiles by sedimentary events and the significance of anaerobic oxidation of methane for the burial of sulfur in marine sediments. Geochim. Cosmochim. Acta 67 (14), 2631–2647.

Hepp, D.A., Mörz, T., Grützner, J., 2006. Pliocene glacial cyclicity in a deep-sea sediment drift (Antarctic Peninsula Pacific Margin). Palaeogeogr., Palaeoclimatol., Palaeoecol. 231 (1–2), 181–198.

Hermoyian, C.S., Owen, R.M., 2001. Late Miocene–early Pliocene biogenic bloom: evidence from low-productivity regions of the Indian and Atlantic Oceans. Paleoceanogr. 16 (1), 95–100.

Hillenbrand, C.-D., Ehrmann, W.U., 2002. Distribution of clay minerals in drift sediments on the continental rise west of the Antarctic Peninsula, ODP Leg 178, Sites 1095 and 1096. In: Barker, P.F., Camerlenghi, A., Acton, G.D., Ramsay, A.T.S. (Eds.), Proc. ODP Sci. Res. Texas A&M University, College Station, TX, pp. 1–29. [CD-ROM].

Hillenbrand, C.-D., Fütterer, D.K., 2002. Neogene to Quaternary deposition of opal on the continental rise west of the Antarctic Peninsula, ODP Leg 178, Sites 1095, 1096, and 1101. In: Barker, P.F., Camerlenghi, A., Acton, G.D., Ramsay, A.T.S. (Eds.), Proc. ODP Sci. Res. Texas A&M University, College Station, TX, pp. 1–33. [CD-ROM].

Hillenbrand, C.-D., Ehrmann, W.U., 2005. Late Neogene to Quaternary environmental changes in the Antarctic Peninsula region: evidence from drift sediments. Glob. Planet. Change 45 (1–3), 165–191.

Hillenbrand, C.-D., Cortese, G., 2006. Polar stratification: a critical view from the Southern Ocean. Palaeogeogr., Palaeoclimatol., Palaeoecol. 242 (3–4), 240–252.

Hillenbrand, C.D., Camerlenghi, A., Cowan, E.A., Hernández-Molina, F.J., Lucchi, R.G., Rebesco, M., Uenzelmann-Neben, G., 2008. The present and past bottom-current flow regime around the sediment drifts on the continental rise west of the Antarctic Peninsula. Mar. Geol. 255 (1–2), 55–63.

Hounslow, M.W., Maher, B.A., 1995. Quantitative extraction and analysis of carriers of magnetization in sediments. Geophys. J. Int. 124 (1), 57–74.

Iwai, M., Acton, G.D., Lazarus, D.B., Osterman, L.E., Williams, T., 2002. Magnetobiochronologic synthesis of ODP Leg 178 rise sediments from the Pacific sector of the Southern Ocean: Sites 1095, 1096, and 1101. In: Barker, P.F., Camerlenghi, A., Acton, G.D., Ramsay, A.T.S. (Eds.), Proc. ODP Sci. Res. Texas A&M University, College Station, TX, pp. 1–40. [CD-ROM].

Karlin, R., 1990. Magnetite diagenesis in marine sediments from the Oregon continental margin. J. Geophys. Res. 95, 4405–4419.

Kasten, S., Zabel, M., Heuer, V., Hensen, C., 2003. Processes and signals of nonsteady-state diagenesis in deep-sea sediments and their pore waters. In: Wefer, G., Mulitza, S., Ratmeyer, V. (Eds.), The South Atlantic in the Late Quaternary. Reconstruction of material budgets and current systems. Springer, Berlin, Heidelberg, New York, pp. 431–459.

Kennett, J.P., Barker, P.F., 1990. Latest Cretaceous to Cenozoic climate and oceanographic developments in the Weddell Sea, Antarctica: an ocean-drilling perspective. In: Barker, P.F., Kennett, J.P. (Eds.), Proc. ODP Sci. Res. Texas A&M University, College Station, TX, pp. 937–960.

Kennett, J.P., Hodell, D.A., 1995. Stability or instability of Antarctic ice sheets during warm climates of the Pliocene? GSA Today 5 (1), 9–13.

Knorr, G., Lohmann, G., 2003. Southern Ocean origin for the resumption of Atlantic thermohaline circulation during deglaciation. Nature 424 (6948), 532–536.

Kumar, N., et al., 1995. Increased biological productivity and export production in the glacial Southern Ocean. Nature 378, 675–680.

Lear, C.H., Elderfield, H., Wilson, P.A., 2000. Cenozoic deep-sea temperatures and global ice volumes from Mg/Ca in benthic Foraminiferal calcite. Science 287, 269–272.

Liebermann, R.C., Banerjee, S.K., 1971. Magnetoelastic interactions in hematite: implications for geophysics. J. Geophys. Res. 76, 2735–2756.

Lucchi, R.G., et al., 2002a. Sedimentary processes and glacial cycles on the sediment drifts of the Antarctic Peninsula Pacific margin: preliminary results of SEDANO-II project. N. Z. J. Geol. Geophys. 35, 275–280.

Lucchi, R.G., et al., 2002b. Mid–late Pleistocene glacimarine sedimentary processes of a high-latitude, deep-sea sediment drift (Antarctic Peninsula Pacific margin). Mar. Geol. 189 (3–4), 343–370.

Lucchi, R.G., Rebesco, M., 2007. Glacial contourites on the Antarctic Peninsula margin: insight for palaeoenvironmental and palaeoclimatic conditions. In: Viana, A.R., Rebesco, M. (Eds.), Economic and Palaeoceanographic Significance of Contourite Deposits. Geological Society special publication. Geological Society, London, pp. 111–127.

Müller, P.J., Schneider, R.R., 1993. An automated leaching method for the determination of opal in sediments and particulate matter. Deep-Sea Res. I 40 (3), 425–444.

Novosel, I., Spence, G.D., Hyndman, R.D., 2005. Reduced magnetization produced by increased methane flux at a gas hydrate vent. Mar. Geol. 216 (4), 265–274.

ODP Leg 165 Shipboard Scientific Party, 1997. Site 998. In: Sigurdsson, H., Leckie, R.M., Acton, G.D. (Eds.), Proceedings of the Ocean Drilling Program, Initial Reports. Texas A&M University, College Station, TX, pp. 49–130.

ODP Leg 178 Shipboard Scientific Party, 1999. Site 1095. In: Barker, P.F., Camerlenghi, A., Acton, G.D. (Eds.), Proceedings of the Ocean Drilling Program, Initial Reports. Texas A&M University, College Station, TX, pp. 1–173. [CD-ROM].

ODP Leg 181 Shipboard Scientific Party, 1999. Site 1124: Rekohu Drift — from the K/T boundary to the deep western boundary current. In: Carter, R.M., McCave, I.N., Richter, C., Carter, L. (Eds.), Proceedings of the Ocean Drilling Program, Initial Reports. Texas A&M University, College Station, TX, pp. 1–137. [CD-ROM].

Passier, H.F., Middelburg, J.J., de Lange, G.J., Bottcher, M.E., 1999. Modes of sapropel formation in the eastern Mediterranean: some constraints based on pyrite properties. Mar. Geol. 153 (1–4), 199–219.

Pudsey, C.J., 2000. Sedimentation on the continental rise west of the Antarctic Peninsula over the last three glacial cycles. Mar. Geol. 167 (3–4), 313–338.

Pudsey, C.J., 2002. Neogene record of Antarctic Peninsula glaciation in continental rise sediments: ODP Leg 178, Site 1095. In: Barker, P.F., Camerlenghi, A., Acton, G.D., Ramsay, A.T.S. (Eds.), Proc. ODP Sci. Res. Texas A&M University, College Station, TX, pp. 1–25. [CD-ROM].

Pudsey, C.J., Camerlenghi, A., 1998. Glacial–interglacial deposition on a sediment drift on the Pacific margin of the Antarctic Peninsula. Ant. Sci. 10 (3), 286–308.

Rebesco, M., Camerlenghi, A., 2008. Late Pliocene margin development and mega debris flow deposits on the Antarctic continental margins: evidence of the onset of the modern Antarctic Ice Sheet? Palaeogeogr., Palaeoclimatol., Palaeoecol. 260 (1–2), 149–167.

Rebesco, M.A., et al., 2002. Sediment drifts and deep-sea channel systems, Antarctic Peninsula Pacific Margin. In: Stow, D.A.V., Pudsey, C.J., Howe, J.A., Faugères, J.C., Viana, A.R. (Eds.), Deep-Water Contourite Systems: Modern Drifts and Ancient Series, Seismic and Sedimentary Characteristics. Geological Society Memoir. Geological Society, London, pp. 353–371.

Rebesco, M., Camerlenghi, A., Geletti, R., Canals, M., 2006. Margin architecture reveals the transition to the modern Antarctic ice sheet ca. 3 Ma. Geology 34 (4), 301–304.

Riedinger, N., et al., 2005. Diagenetic alteration of magnetic signals by anaerobic oxidation of methane related to a change in sedimentation rate. Geochim. Cosmochim. Acta 69 (16), 4117–4126.

Roberts, A., 1995. Magnetic properties of sedimentary greigite (Fe3S4). Earth Planet. Sci. Lett. 134 (3), 227–236.
Sagnotti, L., Macrí, P., Camerlenghi, A., Rebesco, M.A., 2001. Environmental magnetism of Antarctic Late Pleistocene sediments and interhemispheric correlation of climatic events. Earth Planet. Sci. Lett. 192 (1), 65–80.
Talarico, F., Armadillo, E., Ferraccioli, F., Rastelli, N., 2003. Magnetic petrology of the Ross Orogen in Oates Land (Antarctica). Terra Ant. 10, 197–220.
Thomson, J., Jarvis, I., Green, D.R.H., Green, D., 1998. Oxidation fronts in Madeira abyssal plain turbidites: persistence of early diagenetic trace-element enrichments during burial, Site 950. In: Schmincke, H.U., Weaver, P.P.E., Firth, J.V., Duffield, W. (Eds.), Proc. ODP Sci. Res. Texas A&M University, College Station, TX, pp. 559–572.
Uenzelmann-Neben, G., 2006. Depositional patterns at Drift 7, Antarctic Peninsula: along-slope versus down-slope sediment transport as indicators for oceanic currents and climatic conditions. Mar. Geol. 233 (1–4), 49–62.
Vogt, C., Lauterjung, J., Fischer, R.X., 2002. Investigation of the clay fraction (< 2 µm) of the Clay Minerals Society reference clays. Clays Clay Miner. 50 (3), 388–400.
Volpi, V., Camerlenghi, A., Hillenbrand, C.-D., Rebesco, M.A., Ivaldi, R., 2003. Effects of biogenic silica on sediment compaction and slope stability on the Pacific margin of the Antarctic Peninsula. Basin Res. 15 (3), 339–363.
Weeks, R.J., Roberts, A.P., Verosub, K.L., Okada, M., Dubuisson, G.J., 1995. Magnetostratigraphy of upper Cenozoic sediments from Leg 145, North Pacific Ocean. In: Rea, D.K., Basov, I.A., Scholl, D.W., Allan, J.F. (Eds.), Proc. ODP Sci. Res. Texas A&M University, College Station, TX, pp. 491–521.
Weltje, G.J., Tjallingii, R., 2008. Calibration of XRF core scanners for quantitative geochemical logging of sediment cores: theory and application. Earth Planet. Sci. Lett. 274 (3–4), 423–438.
Whitehead, J.M., Wotherspoon, S., Bohaty, S.M., 2005. Minimal Antarctic sea ice during the Pliocene. Geol. 33 (2), 137–140.
Wolf-Welling, T.C.W., Mörz, T., Hillenbrand, C.-D., Pudsey, C.J., Cowan, E.A., 2002. Bulk sediment parameters (CaCO3, TOC, and > 63 µm) of Sites 1095, 1096, and 1101, and coarse-fraction analysis of Site 1095 (ODP Leg 178, western Antarctic Peninsula). In: Barker, P.F., Camerlenghi, A., Acton, G.D., Ramsay, A.T.S. (Eds.), Proc. ODP Sci. Res. Texas A&M University, College Station, TX, pp. 1–19. [CD-ROM].
Zachos, J.C., Pagani, M., Sloan, L., Thomas, E., Billups, K., 2001. Trends, rhythms, and aberrations in global climate 65 ma to present. Science 292, 686–693.